


Article

Efficient Design of Battery Thermal Management Systems for Improving Cooling Performance and Reducing Pressure Drop

Kai Chen ^{1,2} , Ligong Yang ¹, Yiming Chen ¹, Bingheng Wu ^{3,*} and Mengxuan Song ^{4,5,*}

¹ Key Laboratory of Enhanced Heat Transfer and Energy Conservation of the Ministry of Education, School of Chemistry and Chemical Engineering, South China University of Technology, Guangzhou 510640, China; chenkaib09@126.com (K.C.); ligongy@icloud.com (L.Y.); eyminc@outlook.com (Y.C.)

² Jiangsu Province Engineering Laboratory of High Efficient Energy Storage Technology and Equipments, China University of Mining & Technology, Xuzhou 221116, China

³ School of Mechanical and Electrical Engineering, Guangzhou Railway Polytechnic, Guangzhou 511300, China

⁴ Shanghai Key Laboratory of Engineering Materials Application and Evaluation, School of Energy and Materials, Shanghai Polytechnic University, Shanghai 201209, China

⁵ Shanghai Thermophysical Properties Big Data Professional Technical Service Platform, Shanghai Engineering Research Center of Advanced Thermal Functional Materials, Shanghai 201209, China

* Correspondence: wubingheng@gtxy.edu.cn (B.W.); songmx@sspu.edu.cn (M.S.)

Abstract: The air-cooled system is one of the most widely used battery thermal management systems (BTMSs) for the safety of electric vehicles. In this study, an efficient design of air-cooled BTMSs is proposed for improving cooling performance and reducing pressure drop. Combining with a numerical calculation method, a strategy with a varied step length of adjustments (Δd) is developed to optimize the spacing distribution among battery cells for temperature uniformity improvement. The optimization results indicate that the developed strategy reduces the optimization time by about 50% compared with a strategy using identical Δd values while maintaining good performance of the optimized system. Furthermore, the system's pressure drop does not increase after the spacing optimization. Based on this characteristic, a structural design strategy is proposed to improve the cooling performance and reduce the pressure drop simultaneously. First, the appropriate flow pattern is arranged and the secondary outlet is added to reduce the pressure drop of the system. The results show that the BTMS with U-type flow combined with a secondary outlet against the original outlet can effectively reduce the pressure drop of the system. Subsequently, this BTMS is further improved using the developed cell spacing optimization strategy with varied Δd values while the pressure drop is fixed. It is found that the final optimized BTMS achieves a battery temperature difference below 1 K for different inlet airflow rates, with the pressure drop being reduced by at least 45% compared with the BTMS before the optimization.

Keywords: battery thermal management; air cooling; cell spacing; secondary outlet; pressure drop reduction



Citation: Chen, K.; Yang, L.; Chen, Y.; Wu, B.; Song, M. Efficient Design of Battery Thermal Management Systems for Improving Cooling Performance and Reducing Pressure Drop. *Energies* **2024**, *17*, 2275. <https://doi.org/10.3390/en17102275>

Academic Editor: Christopher Micallef

Received: 31 December 2023

Revised: 10 April 2024

Accepted: 17 April 2024

Published: 9 May 2024



Copyright: © 2024 by the authors. Licensee MDPI, Basel, Switzerland. This article is an open access article distributed under the terms and conditions of the Creative Commons Attribution (CC BY) license (<https://creativecommons.org/licenses/by/4.0/>).

1. Introduction

Nowadays, much attention is paid to electric vehicles (EVs) with the increasing threat of environmental pollution and energy crises. Lithium-ion batteries have been widely used in electric vehicles due to the advantages of their capacity, power and energy density, charge retention, life cycle, and competitive cost [1]. However, lithium-ion batteries may release a large amount of heat when working. High temperatures or a large amount of temperature inhomogeneity will damage the battery pack and even cause safety problems [2]. Thus, battery thermal management systems (BTMSs) are essential to quickly dissipate the heat of battery packs.

Designing an appropriate BTMS for EVs is of great concern to many scholars. Various BTMSs have been developed, including the air cooling system [3–5], liquid cooling

system [6–10], phase-change material cooling system [11–13], and hybrid cooling system [14,15], where the air cooling system is one of the most mature solutions, with the advantages of a simple structure, light weight, and low cost [16]. Parametric studies have indicated that the structural parameters are significant factors affecting the performance of air-cooled BTMSs, including the flow pattern, deflector shape, and cell spacing distribution. In recent years, scholars have carried out a lot of research to design the structure of air-cooled BTMSs for performance improvement. Pesaran et al. [17] found that an air-cooled BTMS with a parallel pattern could lower the temperature and improve the temperature uniformity compared with one with a series pattern. Wang et al. [18] investigated the effect of battery cell arrangement on the thermal performance of air-cooled BTMSs, finding that an axisymmetric structure with the fan located on top of the module could lower the temperature and improve the temperature uniformity. Chen et al. [19] homogenized the airflow rates in the parallel channels to improve the performance of parallel BTMSs through adopting a secondary vent. Shi et al. [20] improved the performance of a U-type BTMS with additional vents by adjusting the size and number of the vents. Zhang et al. [21] investigated the impact of the number of secondary outlets on the performance of a Z-type air-cooled system and observed that the system achieved optimal performance when employing six secondary outlets.

In other studies, a tapered cooling duct was introduced into BTMSs with a Z-type flow [22] and U-type flow [23], respectively. The numerical results indicated that the tapered cooling duct improved the temperature uniformity in the battery pack while maintaining its layout. Shahid et al. [24] performed an experiment and also found that the battery temperature difference could be remarkably reduced using a tapered duct in the system. Xie et al. [25] designed the cell spacing distribution, plenum angles, and the inlet and outlet using the orthogonal test method. The optimized solution, respectively, achieved 12.82% and 29.72% reductions for the maximum temperature and temperature difference of the battery pack. Xi et al. [26] added deflectors in the divergence duct and convergence duct in a Z-type BTMS to reduce the maximum temperature and temperature difference. Zhang et al. [27] adopted a binary search method to optimize the inlet deflector angle of an L-type air-cooled system, and their results showed that the maximum temperature and temperature difference in the battery pack were reduced by 1.6 K and 2.0 K after the optimization. However, the design of the deflector shape usually increases the pressure drop of air-cooled BTMSs, leading to more power consumption.

Cell spacing distribution is another critical structural parameter affecting the temperature of a battery pack. Liu et al. [28] developed a shortcut computational model to calculate the temperatures of a battery pack, and used this model to design the plenum angles, the minimal plenum width, and the spacings of the cells. Zhu et al. [29] introduced decreased cell spacings in an air-cooled BTMS, which achieved a significant improvement regarding the temperature uniformity of the system. Chen et al. [30] proposed an optimization strategy developed to be combined with a flow resistance network model for the cell spacing optimization of a system with a Z-type flow, achieving effective cooling performance improvement of the system. Liao et al. [31] established a response surface model, and adopted a multi-variable genetic algorithm to design the channel widths of a system with a U-type flow, remarkably improving the cooling performance. Lyu et al. [32] investigated the optimal deflector angles of an air-cooled BTMS, and used a genetic algorithm to further optimize the battery spacings, remarkably reducing the battery temperature difference. Lan et al. [33] introduced reverse airflow into an air-cooled U-type BTMS and adopted a cuckoo search algorithm to optimize the deflector angles and battery spacings, leading to a remarkable reduction in the battery temperature difference. Ghafoor et al. [34] combined a genetic algorithm with a support vector machine to optimize the parallel channel width distribution in a Z-type air-cooled BTMS, with the objective of minimizing the temperature difference of the battery pack, which reduced the maximum temperature and temperature difference of the battery pack by 3.5 K and more than 70%, respectively.

This survey of the literature has shown some effective structural designs for air-cooled BTMSs. However, the existing works mainly focus on improving the temperature uniformity, but rarely consider reducing the power consumption. In fact, power consumption is a very important index, which affects the cost of the system [35]. Therefore, with the flow rate fixed, an efficient design needs to be conducted to make air-cooled BTMSs achieve good cooling performance and a low pressure drop (power consumption) simultaneously. In this paper, a method for the multi-parameter design of a parallel air-cooled BTMS is investigated. A numerical method is adopted to calculate the flow and temperature fields of the BTMS, and the effectiveness of the results are tested using experimental data. Based on the numerical method, a varied step length of adjustments (Δd) is introduced into the optimization strategy to accelerate the process of cell spacing design. Combining with the developed spacing optimization strategy, the flow pattern of the system is arranged and a secondary outlet is added to further improve the system performance. Finally, typical cases are used to test the cooling efficiency of the designed system.

2. Numerical Method

Calculation Models

Figure 1 shows a typical air-cooled BTMS with a Z-type flow. The maximum temperature (T_{\max}), temperature difference (ΔT_{\max}) of the battery cells, and total pressure drop (ΔP) are the main parameters to describe the BTMS's performance, which are evaluated using a Computational Fluid Dynamics (CFD) method. As the inlet Reynolds number is larger than 2300, the flow in the system is considered to be a turbulent flow. As the temperature differences inside the air and inside the batteries are not large, the physical properties are considered as constants. The radiative and buoyancy effects are ignored. Thus, the forced convective equations with a k - ε turbulence model are adopted, as follows [30]:

$$\frac{\partial u_i}{\partial x_i} = 0 \quad (1)$$

$$\rho_a u_j \frac{\partial u_i}{\partial x_j} = -\frac{\partial p}{\partial x_i} + \frac{\partial}{\partial x_j} \left[(\mu + \mu_t) \frac{\partial u_i}{\partial x_j} \right] \quad (2)$$

$$\rho_a u_j \frac{\partial k}{\partial x_j} = \frac{\partial}{\partial x_j} \left[\left(\mu + \frac{\mu_t}{\sigma_k} \right) \frac{\partial k}{\partial x_j} \right] + \frac{\mu_t}{2} \left(\frac{\partial u_i}{\partial x_j} + \frac{\partial u_j}{\partial x_i} \right)^2 - \rho_a \varepsilon \quad (3)$$

$$\rho_a u_j \frac{\partial \varepsilon}{\partial x_j} = \frac{\partial}{\partial x_j} \left[\left(\mu + \frac{\mu_t}{\sigma_\varepsilon} \right) \frac{\partial \varepsilon}{\partial x_j} \right] + C_1 \frac{\mu_t}{2} \left(\frac{\partial u_i}{\partial x_j} + \frac{\partial u_j}{\partial x_i} \right)^2 \frac{\varepsilon}{k} - C_2 \rho_a \frac{\varepsilon^2}{k} \quad (4)$$

$$\rho_a c_{p,a} \frac{\partial T_a}{\partial t} + \rho_a c_{p,a} u_j \frac{\partial T_a}{\partial x_j} = \frac{\partial}{\partial x_j} \left[\left(\lambda_a + \frac{c_{p,a} \mu_t}{\sigma_T} \right) \frac{\partial T_a}{\partial x_j} \right] \quad (5)$$

$$\rho_b c_{p,b} \frac{\partial T_b}{\partial t} = \frac{\partial}{\partial x_j} \left[\left(\lambda_{b,j} \frac{\partial T_b}{\partial x_j} \right) \right] + \phi_b \quad (6)$$

$$\mu_t = \rho C_\mu \frac{k^2}{\varepsilon} \quad (7)$$

$$C_\mu = 0.09, C_1 = 1.44, C_2 = 1.92, \sigma_k = 1.0, \sigma_\varepsilon = 1.3, \sigma_T = 0.85 \quad (8)$$

where u_i and p are the Reynolds-averaged velocity and pressure, respectively. k and ε are the kinetic energy and corresponding dissipating rate, respectively. ρ , c_p , and λ are the density, specific heat, and thermal conductivity, respectively. μ and μ_t are the kinetic viscosity and the turbulence viscosity, respectively. The subscripts "a" and "b" represent the parameters of the cooling air and battery cell, respectively. The parameters in Equation (8) are the parameters of the k - ε turbulence model.

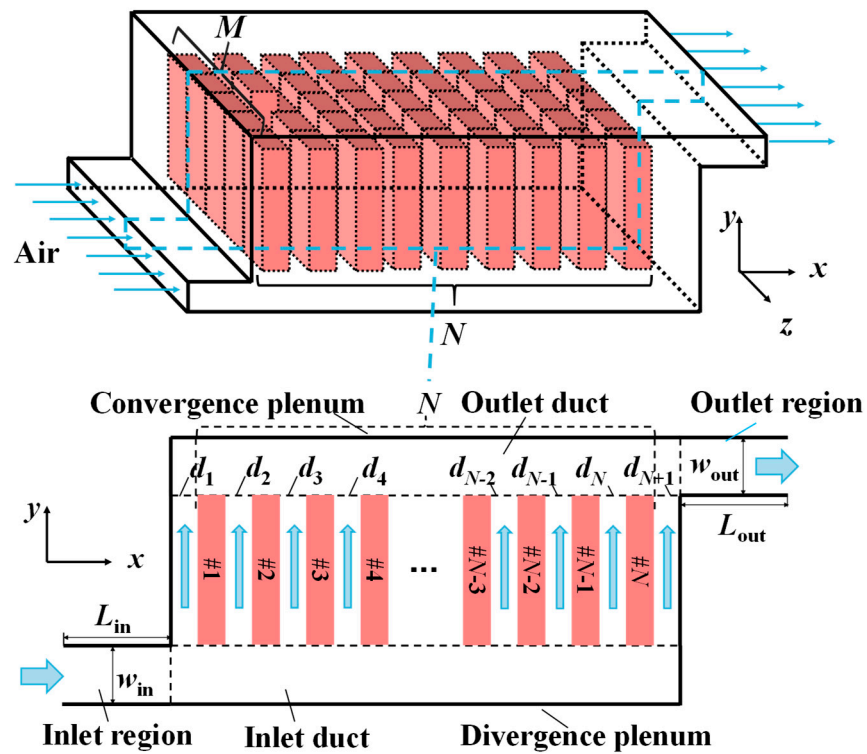


Figure 1. Schematic of the parallel air-cooled BTMS with Z-type flow.

For this study, battery cells with a size of 16 mm × 151 mm × 65 mm and a system described in a previous study [30] were introduced. The parameters of this air-cooled BTMS are shown in Table 1. There are 12 × 2 ($N \times M$) battery cells in this system. The cell spacings are identical to 3.0 mm. A 12 Ah battery was introduced and a 5-current (5C) discharge process was considered. The heat generation model is expressed as follows [30]:

$$\phi_b = \left(I^2 R - IT_b \frac{du}{dT} \right) / V_b \quad (9)$$

$$R = 0.00705 - 0.01853 \times \text{SOC} + 0.05894 \times \text{SOC}^2 - 0.09151 \times \text{SOC}^3 + 0.06579 \times \text{SOC}^4 - 0.01707 \times \text{SOC}^5 \quad (10)$$

where V_b , T_b , I , R , and SOC are the volume, temperature, current, equivalent resistance, and state of charge of the battery cell. du/dT is valued at -0.22 .

Table 1. Calculation parameters for the air-cooled BTMS.

	Parameter	Value
BTMS	Width of the inlet region (mm)	20
	Width of the outlet region (mm)	20
	Length of the inlet region (mm)	100
	Length of the outlet region (mm)	100
Battery cell	Density (kg/m^3)	1542.9
	Specific heat ($\text{J}/(\text{kg}\cdot\text{K})$)	1337
	Thermal conductivity ($\text{W}/(\text{m}\cdot\text{K})$)	1.05, 21.1, 21.1
Cooling air	Density (kg/m^3)	1.165
	Specific heat ($\text{J}/(\text{kg}\cdot\text{K})$)	1005
	Dynamic viscosity ($\text{kg}/(\text{m}\cdot\text{s})$)	1.86×10^{-5}
	Thermal conductivity ($\text{W}/(\text{m}\cdot\text{K})$)	0.0267

The boundary conditions of the governing equations were set as follows. The flow inlet was chosen as $0.015 \text{ m}^3/\text{s}$ and the temperature was set as 298.15 K . The pressure outlet was introduced as the outlet condition. Non-slip and adiabatic conditions were imposed on the surrounding walls. Continuous conditions were imposed on the interfaces between the batteries and air. The initial temperature of the system was set as 298.15 K . Structural grids were used to discretize the domain, and the first layer of grids near the walls were refined to 0.1 mm . The CFD calculations were conducted using the software ANSYS V19.0.

A previous study [36] indicated that the results of two-dimensional (2D) calculations for parallel air-cooled BTMSs were in good consistency with those of the three-dimensional systems. Different grid numbers were considered and a grid dependence analysis was carried out. Figure 2 depicts the numerical results. The results show that the changes in the T_{\max} and ΔT_{\max} values are no more than 0.02 K when the grid number is larger than 5.9×10^4 . Thus, a grid system with 5.9×10^4 cells was adopted when conducting the simulation.

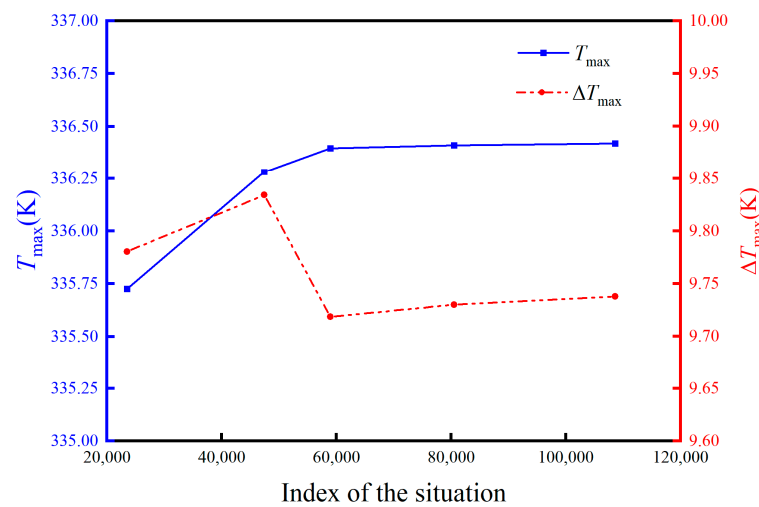


Figure 2. Results of the grid dependence analysis.

3. Cell Spacing Optimization

3.1. Cell Spacing Optimization Process

Previous studies have demonstrated that cell spacing optimization is effective to improve the temperature uniformity of battery packs in air-cooled BTMSs [37]. Thus, an optimization strategy that adjusts the spacing distribution step by step was developed. For a specified channel, the pressure drop is reduced when the width of this channel is increased, and more air will flow through this channel to reduce the temperatures of the cells beside this channel, and vice versa. Therefore, the width of the channel (cell spacing) around the battery cell with a high temperature should be increased, while that around the battery cell with a low temperature should be reduced [37]. During the adjusting process, an identical step length of adjustments (Δd) was used. The results indicated that a smaller Δd achieved a better solution, but needed a longer optimization time. In this section, a strategy with varied Δd is developed to shorten the time of cell spacing optimization. The variable \mathbf{W} is introduced to represent the spacing distribution of the battery cells, shown as

$$\mathbf{W} = [d_1, d_2, \dots, d_i, \dots, d_{N+1}] \quad (11)$$

where d_i represents the spacing between the $(i - 1)$ th and the i th cells, and N represents the number of battery cells. A varied Δd was used during the optimization process, and the detailed steps are listed as follows:

1. The initial spacing distribution is set as $\mathbf{W}_{\text{initial}}$, and the varied Δd sequence (\mathbf{D}) is set as $[\Delta d_1, \Delta d_2, \dots, \Delta d_i, \dots, \Delta d_n]$, where n is the number of Δd values and $\Delta d_i > \Delta d_{i+1} > 0$. Let the spacing distribution $\mathbf{W} = \mathbf{W}_{\text{initial}}$ and the step length $\Delta d = \Delta d_1$.

2. Evaluate the performance of the BTMS with \mathbf{W} using the CFD method, obtaining the value of ΔT_{\max} . Record the minimum ΔT_{\max} during the optimization process as ΔT_{opt} , and the relevant spacing distribution as \mathbf{W}_{opt} .
3. Change \mathbf{W} through the following strategy: Find the index of the channel between the battery cells with maximum temperatures, denoted as n_{\max} . Find the index of the channel between the battery cells with minimum temperatures, denoted as n_{\min} . Let $d_{n_{\max}} = d_{n_{\max}} + \Delta d$ and $d_{n_{\min}} = d_{n_{\min}} - \Delta d$.
4. After conducting Step 3, a new \mathbf{W}' value is obtained. Evaluate the performance of the system with \mathbf{W}' , obtaining the relevant battery temperature difference, denoted as $\Delta T'_{\max}$. If $\Delta T'_{\max} < \Delta T_{\text{opt}}$, let $\Delta T_{\text{opt}} = \Delta T'_{\max}$ and $\mathbf{W}_{\text{opt}} = \mathbf{W}'$.
5. If ΔT_{opt} is not reduced while continuing to adjust \mathbf{W} , Δd is reduced to the next value in the sequence \mathbf{D} . Let $\mathbf{W} = \mathbf{W}'$, and return to Step 3. If Δd is the last one in \mathbf{D} , the process is stopped, and \mathbf{W}_{opt} is the final optimized solution.

3.2. Optimization Results

For this section, spacing optimization was conducted using the developed strategy for a typical BTMS. Before optimization, the system with identical cell spacings is denoted as BTMS Z. Considering the varied Δd values of [1.0, 0.5, 0.2, 0.1] mm, the final solution is denoted as BTMS Zopt. Optimizations with identical Δd values at 1.0 mm, 0.5 mm, and 0.2 mm were also conducted, respectively. The solutions are, respectively, denoted as BTMSs Zopt-1, Zopt-0.5, and Zopt-0.2. For each situation, $\mathbf{W}_{\text{initial}}$ is set as the identical spacing distribution.

Figure 3 depicts the ΔT_{\max} values with the spacing adjustment step. Table 2 lists the optimized results for various situations. It is noticed that the widths of the second channel are much larger than the others for the optimized cell spacing distribution. This is because the temperature of battery #1 is the highest in BTMS Z, and a large width in the second channel will increase the flow rate around battery #1 to reduce the maximum temperature. For the situations with identical Δd values, the number of the adjustment steps (N_a) corresponding to the final solution increases as Δd decreases. N_a of BTMS Zopt-0.2 is about five times as high as that of BTMS Zopt-1, and is about twice as high as that of Zopt-0.5. However, BTMS Zopt-0.2 performed much better than BTMSs Zopt-1 and Zopt-0.5. ΔT_{\max} of BTMS Zopt-0.2 was, respectively, 58% and 42% lower than those of BTMSs Zopt-1 and Zopt-0.5. Compared with the optimized system with identical Δd values, the one with varied Δd values can achieve a good solution in a shorter time. T_{\max} and ΔT_{\max} of BTMS Zopt were almost the same as those of BTMS Zopt-0.2, but N_a was only 24, which was half of that of BTMS Zopt-0.2. The results in Figure 3 indicate that a larger Δd can make ΔT_{\max} decrease more quickly at the beginning of the optimization process, and a smaller Δd can make ΔT_{\max} further decrease to find a better solution at the end. Therefore, varying Δd from a large value to a small value can help to achieve a good solution in a short time. Moreover, compared to BTMS Z, T_{\max} and ΔT_{\max} in BTMS Z-opt were reduced by 3.9 K and 8.6 K, respectively. The results also demonstrate that the total pressure drop of the system did not increase for different optimized BTMSs. This conclusion is similar to that found in a previous study [37]. In summary, the strategy with varied step lengths is better than the one with identical step lengths, which can effectively shorten the time of cell spacing optimization while maintaining a good cooling performance and pressure drop of the solution.

Table 2. The optimized results of various Δd values ($Q_0 = 0.015 \text{ m}^3/\text{s}$).

BTMS	N_a	\mathbf{W} (mm)	T_{\max} (K)	ΔT_{\max} (K)	ΔP (Pa)
Z	–	[3.0, 3.0, 3.0, 3.0, 3.0, 3.0, 3.0, 3.0, 3.0, 3.0, 3.0, 3.0, 3.0]	336.4	9.7	47.34
Zopt-1	8	[3.0, 8.0, 3.0, 3.0, 3.0, 3.0, 2.0, 3.0, 2.0, 3.0, 2.0, 3.0, 1.0]	332.8	3.1	46.10
Zopt-0.5	21	[3.0, 9.5, 2.5, 3.5, 2.5, 3.0, 2.5, 2.5, 2.0, 2.5, 1.5, 3.0, 1.0]	333.3	2.3	45.90
Zopt-0.2	49	[3.0, 10.2, 2.2, 3.8, 2.4, 2.8, 2.2, 2.6, 2.0, 2.4, 1.8, 2.4, 1.2]	332.4	1.3	45.95
Zopt	24	[3.0, 9.4, 2.3, 3.8, 2.3, 3.0, 2.3, 2.6, 1.9, 2.8, 1.6, 3.0, 1.0]	332.5	1.1	45.89

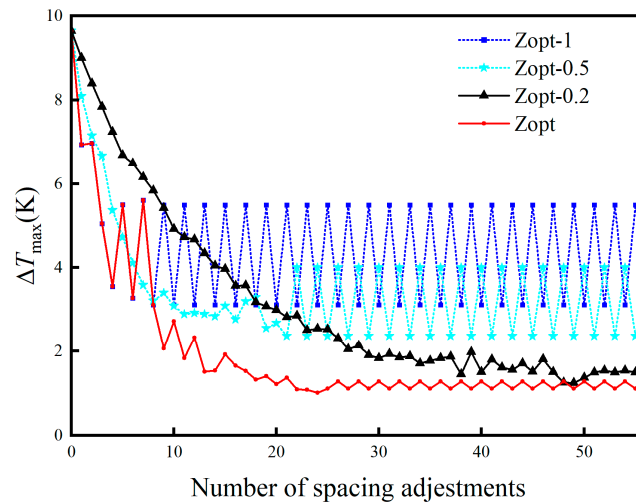


Figure 3. ΔT_{\max} with the spacing adjustment process for BTMS Z.

4. Improvement of the System's Performance

The results in Section 3.2 indicate that the cell spacing design does not increase the total pressure drop of an air-cooled BTMS. Therefore, this study reduced the system's pressure drop through changing the system structure. Then, cell spacing optimization was conducted using the strategy with varied Δd values to improve the temperature uniformity without increasing the pressure drop. The final solution is expected to achieve a small battery temperature difference with a low pressure drop.

4.1. Improvement through Changing the Flow Pattern

A previous study [36] indicated that a BTMS with a U-type flow (denoted as BTMS U) achieved a smaller pressure drop than BTMS Z. In this section, the proposed strategy with varied Δd values is used to design the cell spacing distribution of BTMS U. Figure 4 depicts the schematic of BTMS U. Table 3 lists the performances of BTMS U and the relevant spacing-optimized BTMS (denoted as BTMS Uopt). We can see that it only performs 15 adjusting steps to achieve the optimized result. The result shows that the spacing distribution of BTMS Uopt is different from that of BTMS Zopt. As the temperatures of the battery cells far from the inlet are higher than those near the inlet in BTMS U, the widths of the parallel channels far from the inlet tend to increase for BTMS Uopt. Again, the optimized result of BTMS U demonstrates the effectiveness of cell spacing optimization for BTMS U. Compared with BTMS U, ΔT_{\max} in BTMS Uopt decreased by 81% without increasing T_{\max} and ΔP . Furthermore, the T_{\max} and ΔT_{\max} values of BTMS Uopt were similar to those of BTMS Zopt, but the pressure drop was 11% lower. Therefore, BTMS Uopt achieves better cooling efficiency than BTMS Zopt.

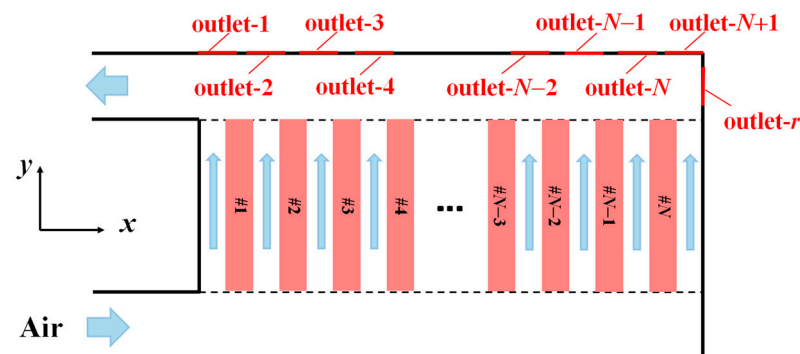


Figure 4. Schematic of BTMS U with a secondary outlet.

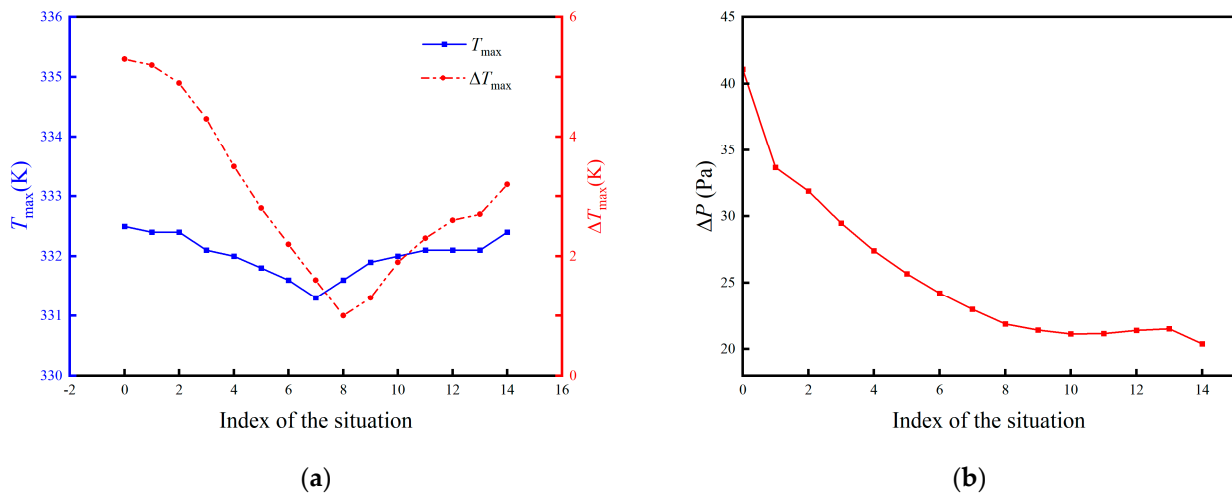
Table 3. Optimized results of the BTMS with a U-type flow ($Q_0 = 0.015 \text{ m}^3/\text{s}$).

BTMS	N_a	W (mm)	T_{\max} (K)	ΔT_{\max} (K)	ΔP (Pa)
U	-	[3.0, 3.0, 3.0, 3.0, 3.0, 3.0, 3.0, 3.0, 3.0, 3.0, 3.0, 3.0, 3.0]	332.5	5.3	41.07
Uopt	15	[1.0, 4.6, 1.9, 3.5, 2.4, 3.1, 2.9, 3.0, 3.2, 3.1, 3.5, 3.8, 3.0]	332.3	1.0	40.62

4.2. Improvement through Adding a Secondary Outlet

Previous research has shown that the pressure drop of a parallel BTMS can be reduced through adding a secondary airflow outlet [19]. For this section, a secondary outlet was added into BTMS U to find a BTMS with a lower pressure drop. Then, cell spacing optimization was conducted for the system with the secondary outlet to further reduce ΔT_{\max} with the pressure drop fixed.

Various positions of the secondary outlet were considered, as shown in Figure 4. For each situation, the secondary outlet was against one of the cooling channels. The width and the length of the secondary outlet region were set as 20 mm and 100 mm, respectively. For convenience, the BTMS with a secondary outlet against the i th cooling channel is represented as BTMS U- i . Moreover, a situation with the secondary outlet against the original outlet was also considered, denoted as BTMS U-r. Figure 5 shows comparisons of the values of T_{\max} , ΔT_{\max} , and ΔP for the BTMSs with the secondary outlet at different positions. In Figure 5, the horizontal axis represents the position of the secondary outlet, where “0” stands for BTMS U and “14” stands for BTMS U-r. From Figure 5a, it can be observed that the secondary outlet can effectively improve the performance of BTMS U. BTMS U-8 achieved the smallest ΔT_{\max} among the various systems. ΔT_{\max} of BTMS U-8 with identical cell spacings is only 1.0 K, similar to those of BTMSs Zopt and Uopt. ΔP was also reduced effectively through adding the secondary outlet, as shown in Figure 5b. This is because some of the cooling air leaves the system from the secondary outlet before going through the whole duct. Referred to the ΔP values, BTMS U-r achieved the best performance. The ΔP values of BTMS U-r were 50% lower and 57% lower than BTMSs U and Z, respectively.

**Figure 5.** Performances of the BTMSs with a secondary outlet at different positions. (a) T_{\max} and ΔT_{\max} . (b) ΔP .

Based on the aforementioned analysis, cell spacing optimizations were conducted for BTMSs U-8 and U-r, respectively. The optimized solutions are shown in Table 4. The optimized systems for the two situations are represented as BTMSs Uopt-8 and Uopt-r, respectively. Similarly, we find that the developed optimization strategy can remarkably improve the temperature uniformity of the battery pack. Compared with those of BTMS U-r, T_{\max} of BTMS Uopt-r is 1.5 K lower and ΔT_{\max} is 75% lower. The ΔT_{\max} values of BTMSs

Uopt-8 and Uopt-r are both only 0.4 K. The cooling performances of the two optimized BTMSs are similar, but ΔP of BTMS Uopt-r is 9% lower than that of BTMS Uopt-8. In summary, BTMS Uopt-r achieves a higher cooling efficiency than BTMS Uopt-8.

Table 4. Optimized results of BTMSs U-8 and U-r ($Q_0 = 0.015 \text{ m}^3/\text{s}$).

BTMS	N_a	W (mm)	T_{\max} (K)	ΔT_{\max} (K)	ΔP (Pa)
U-8	—	[3.0, 3.0, 3.0, 3.0, 3.0, 3.0, 3.0, 3.0, 3.0, 3.0, 3.0, 3.0, 3.0]	331.4	1.0	21.87
U-r	—	[3.0, 3.0, 3.0, 3.0, 3.0, 3.0, 3.0, 3.0, 3.0, 3.0, 3.0, 3.0, 3.0]	332.4	3.2	20.39
Uopt-8	6	[2.0, 3.7, 2.9, 3.2, 3.0, 3.0, 3.0, 2.8, 3.1, 2.8, 3.5, 3.0, 3.0]	331.1	0.4	22.07
Uopt-r	5	[3.0, 3.0, 3.9, 3.0, 3.5, 3.1, 3.2, 3.0, 2.9, 3.0, 2.6, 3.0, 1.8]	330.9	0.4	20.11

Figure 6a compares the flow rates among the channels in BTMSs Z, Zopt, Uopt, and Uopt-r. For BTMS Z, as the flow rates of the parallel channels downstream are much larger than those of the channels upstream, the temperatures of the battery cells downstream are lower than those upstream, leading to a large temperature difference in the battery pack (Figure 6b). For the optimized BTMSs, as the air in the channels on both ends only cools one battery, the flow rates in these two channels are smaller than the flow rates in the other channels, which can reduce the battery temperature difference. For the middle channels, BTMS Uopt-r achieves a much more uniform airflow rate distribution than the other BTMSs. Therefore, the battery cell temperatures in BTMS Uopt-r are more uniform than those of BTMSs Zopt and Uopt. Figure 7 depicts the temperature contours of the different systems. It can be observed that BTMSs Zopt and Uopt achieve more uniform temperature distributions than BTMSs Z and U, respectively. The temperature distributions in the battery pack for BTMSs Uopt-8 and Uopt-r are similar, and are more uniform than other systems.

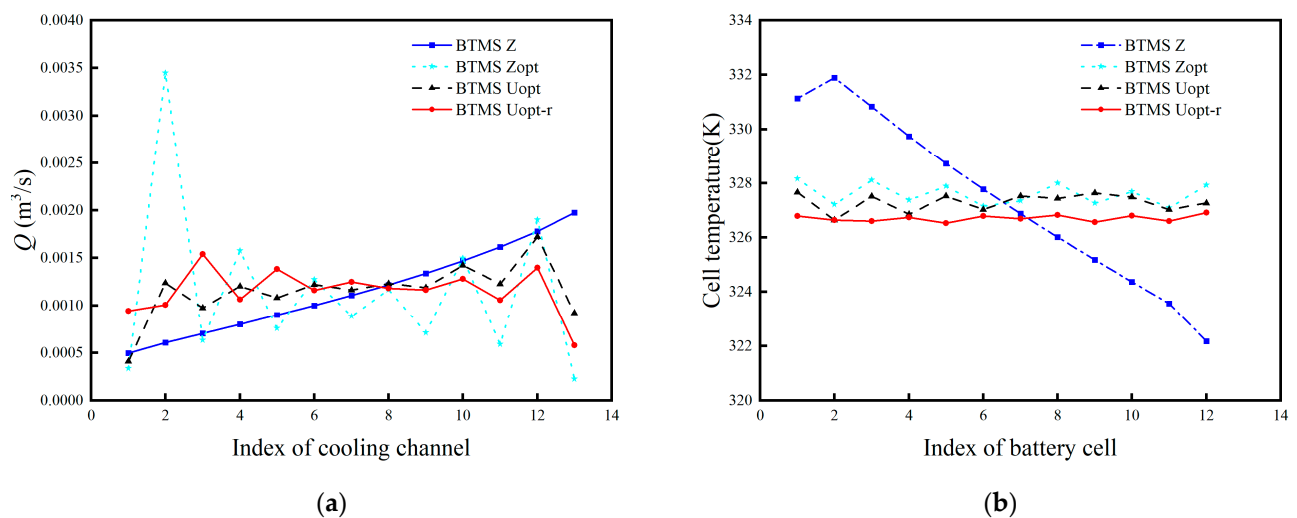


Figure 6. Comparison of the performances of various optimized BTMSs ($Q_0 = 0.015 \text{ m}^3/\text{s}$). (a) Airflow rates in the cooling channels. (b) Cell temperatures.

Furthermore, situations with different airflow rates were considered, and relevant calculations were carried out. Table 5 lists the numerical results for these various situations. It can be observed that the cooling performance of BTMS Uopt was better than that of BTMS Zopt for different flow rates, and the ΔP values of BTMS Uopt were at least 8% lower. BTMS Uopt-r still performed the best of the four BTMSs. For different flow rates, the values of ΔT_{\max} in BTMS Uopt-r remained below 1 K. Compared with BTMS Z, T_{\max} and ΔT_{\max} in BTMS Uopt-r were, respectively, reduced by at least 4.0 K and 7.1 K for the various situations. The reduction rates for ΔT_{\max} and ΔP reached 87% and 51% or more. Compared with BTMS Uopt, T_{\max} in BTMS Uopt-r was reduced by about 1.0 K, and ΔT_{\max}

was 38% lower, with ΔP achieving at least a 45% reduction. In summary, by arranging the flow pattern, adding a secondary outlet at an appropriate position, and conducting cell spacing optimization, the temperature uniformity in the battery pack and the pressure drop of air-cooled BTMSs can be effectively improved simultaneously.

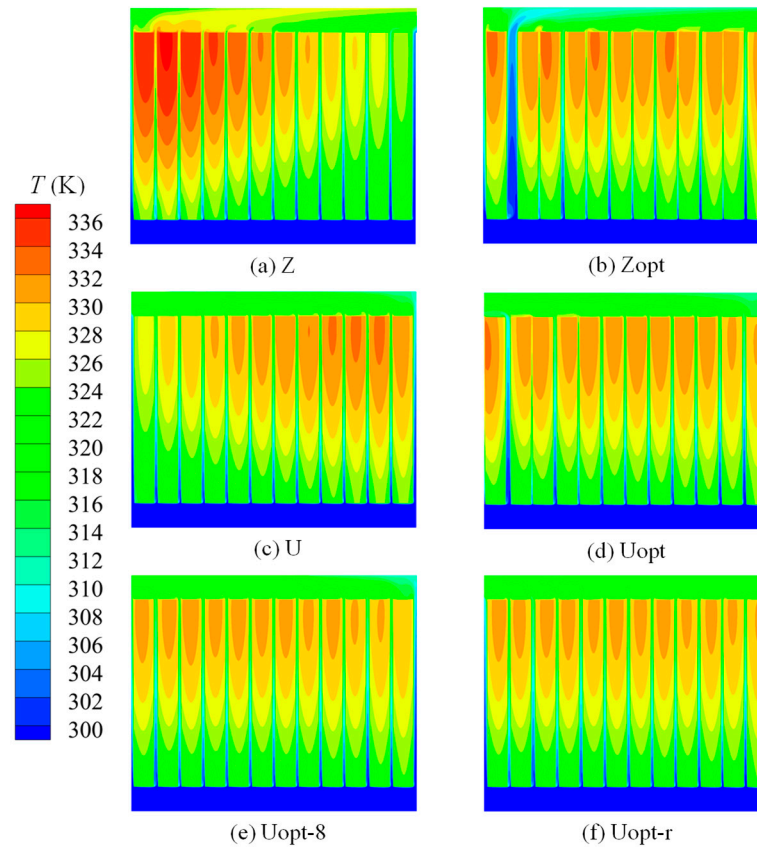


Figure 7. Temperature contours of the different systems.

Table 5. Performances of the BTMSs under various inlet airflow rates.

BTMS	$Q_0 = 0.010 \text{ m}^3/\text{s}$			$Q_0 = 0.015 \text{ m}^3/\text{s}$			$Q_0 = 0.020 \text{ m}^3/\text{s}$		
	T_{\max} (K)	ΔT_{\max} (K)	ΔP (Pa)	T_{\max} (K)	ΔT_{\max} (K)	ΔP (Pa)	T_{\max} (K)	ΔT_{\max} (K)	ΔP (Pa)
Z	338.8	8.1	22.96	336.4	9.7	47.34	334.6	10.8	80.75
Zopt	337.1	2.7	21.90	332.5	1.1	45.89	331.1	3.2	78.92
Uopt	336.3	1.7	20.24	332.3	1.0	40.62	328.8	1.6	67.87
Uopt-r	334.8	1.0	11.22	330.9	0.4	20.11	328.3	0.7	31.19

5. Experimental Validation

Experiments were carried out to validate the accuracy of the numerical results. An air-cooled system with a J-type flow was established, as depicted in Figure 8. This experimental system contained eight aluminum blocks. Each was equipped with three heating rods to simulate the heating generation of the battery cell. The power of the heating rods was controlled using a DC power supply (KXN-645D). Grease was applied between the aluminum blocks and the heating rods to reduce the contact thermal resistance. K-type thermocouples were placed at the center of each aluminum block to measure the local temperature. The specific measurement points are shown in Figure 8, where $T_1 \sim T_8$ represent the temperatures of the measuring points at the aluminum blocks, and T_0 represents the ambient temperature. The temperature data were collected using data acquisition equipment (Agilent 34970A, America). The structural parameters of the experimental system and the properties of the aluminum blocks are listed in Table 6. The air was supplied using a fan.

The inlet velocity of the air was set to 3 m/s. The heating power applied to each aluminum block was 12 W. 2D Numerical calculations were also carried out for the experimental system. A comparison between the numerical results and experimental data was conducted. The ambient temperature was 298.8 K. The highest temperature and temperature difference of the measurement points in the experiments were 328.5 K and 2.1 K, respectively, and those from the simulation were 329.1 K and 1.9 K, respectively. The deviations between the simulation and experiment results were 0.6 K and 0.2 K, respectively. These results indicate a good consistency between the 2D CFD results and the experimental data, which verifies the effectiveness of 2D CFD calculations for parallel air-cooled systems.

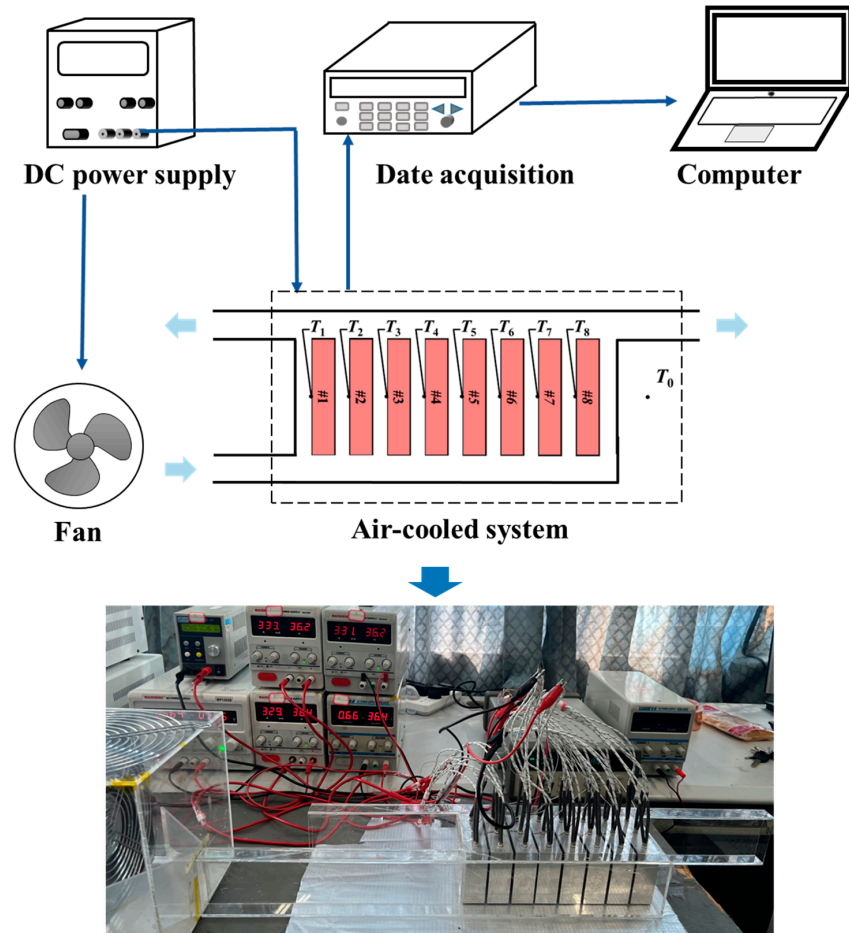


Figure 8. Scheme of the experimental system.

Table 6. Parameters of the air-cooled experimental system.

	Parameter	Value
Experimental system	Width of the inlet region (mm)	20
	Width of the outlet region (mm)	20
	Length of the inlet region (mm)	300
	Length of the outlet region (mm)	300
	Width of parallel channel (mm)	3
	Number of aluminum blocks	8
	Number of parallel channels	9
Aluminum block	Density (kg/m ³)	2700
	Specific heat (J/(kg·K))	900
	Thermal conductivity (W/(m·K))	240
	Size (mm)	27 × 90 × 70

6. Conclusions

In this paper, an efficient design method is used to simultaneously improve the heat dissipation performance and reduce the pressure drop of a parallel BTMS. Combined with a numerical method, a strategy employing a varied step length of adjustments (Δd) is proposed to design the cell spacing distribution in the system. The results indicate that the developed strategy can effectively speed up the cell spacing optimization process. The optimization time using varied Δd values was reduced by about 50% compared with that using small identical Δd values, without worsening the performance of the optimized system. The results also demonstrate that the cell spacing optimization did not change the system's pressure drop. Based on this characteristic, the pressure drop of the system was reduced through choosing the appropriate flow pattern and adding a secondary outlet, and then the cooling performance of the system was improved by optimizing the cell spacing distribution. Finally, a spacing-optimized BTMS with a secondary outlet against the original outlet (BTMS Uopt-r) was designed. This designed system achieved a temperature difference of no more than 1 K, and the pressure drops of BTMS Uopt-r were at least 45% lower than the ones of BTMS Uopt for different inlet airflow rates.

In summary, the developed strategy with a varied step length of adjustments can shorten the time of cell spacing design while maintaining the optimized system's performance. The temperature uniformity and the pressure drop of parallel air-cooled BTMSs can be remarkably improved through choosing the appropriate flow pattern, adding a secondary outlet, and designing the cell spacing distribution.

Author Contributions: K.C.: writing—original draft preparation, data curation, funding acquisition, investigation, software, writing—review and editing. L.Y.: data curation, validation, writing—review and editing. Y.C.: software, writing—review and editing. B.W.: conceptualization, writing—review and editing. M.S.: conceptualization, methodology, writing—review and editing. All authors have read and agreed to the published version of the manuscript.

Funding: This research was supported by the National Natural Science Foundation of China (Grants No. 52276063 and No. 51976062), and the Project of Shanghai Municipal Science and Technology Commission (22DZ2291100).

Data Availability Statement: The data presented in this study are available on request from the corresponding author.

Conflicts of Interest: The authors declare no conflicts of interest.

Nomenclature

c_p	specific heat, J/(kg·K)
C_d	dimensionless friction factor, 1
Δd	step length of cell spacing adjustments, m
D	equivalent diameter of a channel, m
I	charge/discharge current, A
k	turbulent kinetic energy, m^2/s^2
l	length of a channel, m
L_{in}	length of the inlet region of the BTMS, m
L_{out}	length of the outlet region of the BTMS, m
M	raw number of the battery cells, 1
N	column number of the battery cells, 1
p	pressure, Pa
ΔP	pressure drop, Pa
Q	airflow rate, m^3/s
Q_0	inlet airflow rate, m^3/s
R	equivalent resistance of the battery cell, ω
Re	Reynolds number, 1
SOC	state of charge for the battery cell, 1

t	time, s
T	temperature, K
T_{\max}	maximum temperature of the battery pack, K
ΔT_{\max}	temperature difference among the battery cells, K
u_i	i th component of the velocity, m/s
w_{in}	width of the inlet of the BTMS, m
w_{out}	width of the outlet of the BTMS, m
Greek symbols	
λ	thermal conductivity, W/(m·K)
μ	dynamic viscosity of air, Pa·s
ϕ	heat source intensity, W/m ³
ρ	density of air, kg/m ³
$\sigma_k, \sigma_\epsilon, \sigma_T$	parameters of the k - ϵ model, 1
ϵ	turbulent kinetic energy dissipating rate, m ² /s ³
ζ	local loss coefficient, 1
Subscripts	
a	air
b	battery cell
opt	optimized result

References

- Karimi, G.; Li, X. Thermal management of lithium-ion batteries for electric vehicles. *Int. J. Energy Res.* **2013**, *37*, 13–24. [\[CrossRef\]](#)
- Chavan, S.; Venkateswarlu, B.; Prabakaran, R.; Salman, M.; Joo, S.; Choi, G.; Kim, S. Thermal runaway and mitigation strategies for electric vehicle lithium-ion batteries using battery cooling approach: A review of the current status and challenges. *J. Energy Storage* **2023**, *72*, 108569. [\[CrossRef\]](#)
- Xu, X.; Sun, X.; Hu, D.; Li, R.; Tang, W. Research on heat dissipation performance and flow characteristics of air-cooled battery pack. *Int. J. Energy Res.* **2018**, *42*, 3658–3671. [\[CrossRef\]](#)
- Nguyen, T.D.; Deng, J.; Robert, B.; Chen, W.; Siegmund, T. Experimental investigation on cooling of prismatic battery cells through cell integrated features. *Energy* **2022**, *244*, 122580. [\[CrossRef\]](#)
- Chavan, S.; Rudrapati, R.; Venkateswarlu, B.; Joo, S.; Kim, S. An innovative approach to multi-response optimization of battery thermal management systems using multi-desirability function approach. *Appl. Therm. Eng.* **2024**, *236*, 121835. [\[CrossRef\]](#)
- Xie, J.; Mo, C.; Zhang, G.; Yang, X. Thermal performance analysis of liquid cooling system with hierarchically thermal conductive skeleton for large-scaled cylindrical battery module in harsh working conditions. *Int. J. Heat Mass Transf.* **2023**, *215*, 124487. [\[CrossRef\]](#)
- Rao, Z.; Qian, Z.; Kuang, Y.; Li, Y. Thermal performance of liquid cooling based thermal management system for cylindrical lithium-ion battery module with variable contact surface. *Appl. Therm. Eng.* **2017**, *123*, 1514–1522. [\[CrossRef\]](#)
- Wang, C.; Zhang, G.; Meng, L.; Li, X.; Situ, W.; Lv, Y.; Rao, M. Liquid cooling based on thermal silica plate for battery thermal management system. *Int. J. Energy Res.* **2017**, *41*, 2468–2479. [\[CrossRef\]](#)
- Sirikasemsuk, S.; Naphon, N.; Eiamsa-ard, S.; Naphon, P. Analysis of nanofluid flow and heat transfer behavior of Li-ion battery modules. *Int. J. Heat Mass Transf.* **2023**, *208*, 124058. [\[CrossRef\]](#)
- Chavan, S.; Liu, J.; Venkateswarlu, B.; Joo, S.; Kim, S. Numerical simulation of lithium-ion battery thermal management systems: A comparison of fluid flow channels and cooling fluids. *J. Energy Storage* **2023**, *73*, 108940. [\[CrossRef\]](#)
- Samimi, F.; Babapoor, A.; Azizi, M.; Karimi, G. Thermal management analysis of a li-ion battery cell using phase change material loaded with carbon fibers. *Energy* **2016**, *96*, 355–371. [\[CrossRef\]](#)
- Deng, J.; Huang, Q.; Li, X.; Zhang, G.; Li, C.; Li, S. Influence mechanism of battery thermal management with flexible flame retardant composite phase change materials by temperature aging. *Renew. Energy* **2024**, *222*, 119922. [\[CrossRef\]](#)
- Zhang, X.; Su, G.; Lin, J.; Liu, A.; Wang, C.; Zhuang, Y. Three-dimensional numerical investigation on melting performance of phase change material composited with copper foam in local thermal non-equilibrium containing an internal heater. *Int. J. Heat Mass Transf.* **2021**, *170*, 121021. [\[CrossRef\]](#)
- Zeng, W.; Niu, Y.; Li, S.; Hu, S.; Mao, B.; Zhang, Y. Cooling performance and optimization of a new hybrid thermal management system of cylindrical battery. *Appl. Therm. Eng.* **2022**, *217*, 119171. [\[CrossRef\]](#)
- Chen, K.; Huang, Q.; Li, Q.; Liang, S.; Wu, X. Optimization strategy for battery thermal management system with phase change materials, aerogel and cold plates. *Int. J. Heat Mass Transf.* **2024**, *221*, 125070. [\[CrossRef\]](#)
- Wang, H.; Ma, L. Thermal management of a large prismatic battery pack based on reciprocating flow and active control. *Int. J. Heat Mass Transfer.* **2017**, *115*, 296–303. [\[CrossRef\]](#)
- Pesaran, A.A. Battery thermal models for hybrid vehicle simulations. *J. Power Sources* **2002**, *110*, 377–382. [\[CrossRef\]](#)

18. Wang, T.; Tseng, K.J.; Zhao, J.; Wei, Z. Thermal investigation of lithium-ion battery module with different cell arrangement structures and forced air-cooling strategies. *Appl. Energy* **2014**, *134*, 229–238. [[CrossRef](#)]
19. Hong, S.; Zhang, X.; Chen, K.; Wang, S. Design of flow configuration for parallel air-cooled battery thermal management system with secondary vent. *Int. J. Heat Mass Transf.* **2018**, *116*, 1204–1212. [[CrossRef](#)]
20. Shi, Y.; Ahmad, S.; Liu, H.; Lau, K.T.; Zhao, J. Optimization of air-cooling technology for LiFePO₄ battery pack based on deep learning. *J. Power Sources* **2021**, *497*, 229894. [[CrossRef](#)]
21. Zhang, F.; Liu, P.; He, Y.; Li, S. Cooling performance optimization of air cooling lithium-ion battery thermal management system based on multiple secondary outlets and baffle. *J. Energy Storage* **2022**, *52*, 104678. [[CrossRef](#)]
22. Park, H. A design of air flow configuration for cooling lithium ion battery in hybrid electric vehicles. *J. Power Sources* **2013**, *239*, 30–36. [[CrossRef](#)]
23. Sun, H.; Wang, X.; Tossan, B.; Dixon, R. Three-dimensional thermal modeling of a lithium-ion battery pack. *J. Power Sources* **2012**, *206*, 349–356. [[CrossRef](#)]
24. Shahid, S.; Agelin-Chaab, M. Experimental and numerical studies on air cooling and temperature uniformity in a battery pack. *Int. J. Energy Res.* **2018**, *42*, 2246–2262. [[CrossRef](#)]
25. Xie, J.; Ge, Z.; Zang, M.; Wang, S. Structural optimization of lithium-ion battery pack with forced air cooling system. *Appl. Therm. Eng.* **2017**, *126*, 583–593. [[CrossRef](#)]
26. Xi, Y.; Feng, Y.; Xiao, Y.; He, G. Novel Z-shaped structure of lithium-ion battery packs and optimization for thermal management. *J. Energy Eng.* **2020**, *146*, 04019035. [[CrossRef](#)]
27. Zhang, X.; Fan, X.; Deng, Y. Cooling performance optimization of air-cooled battery thermal management system with I-type flow. *Energy Technol.* **2023**, *11*, 2300382. [[CrossRef](#)]
28. Liu, Z.; Wang, Y.; Zhang, J.; Liu, Z. Shortcut computation for the thermal management of a large air-cooled battery pack. *Appl. Therm. Eng.* **2014**, *66*, 445–452. [[CrossRef](#)]
29. Zhu, H.; Zhang, Y.; Zhu, C.; Chen, L. Study of electric vehicle battery thermal management system. *Res. Explor. Lab.* **2011**, *30*, 8–14. (In Chinese)
30. Chen, K.; Song, M.; Wei, W.; Wang, S. Design of the structure of battery pack in parallel air-cooled battery thermal management system for cooling efficiency improvement. *Int. J. Heat Mass Transf.* **2019**, *132*, 309–321. [[CrossRef](#)]
31. Liao, X.; Ma, C.; Peng, X.; Garg, A.; Bao, N. Temperature distribution optimization of an air-cooling lithium-ion battery pack in electric vehicles based on the response surface method. *J. Electrochem. Energy Convers. Storage* **2019**, *16*, 041002. [[CrossRef](#)]
32. Lyu, C.; Song, Y.; Wang, L.; Ge, Y.; Xiong, R.; Lan, T. A new structure optimization method for forced air-cooling system based on the simplified multi-physics model. *Appl. Therm. Eng.* **2021**, *198*, 117455. [[CrossRef](#)]
33. Lan, X.; Li, X.; Ji, S.; Gao, C.; He, Z. Design and optimization of a novel reverse layered air-cooling battery management system using U and Z type flow patterns. *Int. J. Energy Res.* **2022**, *46*, 14206–14226. [[CrossRef](#)]
34. Ghafoor, U.; Yaqub, M.W.; Qureshi, M.U.; Khan, M.N.A. Thermal optimization of Li-ion battery pack using genetic algorithm integrated with machine learning. *Therm. Sci. Eng. Prog.* **2023**, *44*, 102069. [[CrossRef](#)]
35. Zeng, X.; Ge, Y.; Shen, J.; Zeng, L.; Liu, Z.; Liu, W. The optimization of channels for a proton exchange membrane fuel cell applying genetic algorithm. *Int. J. Heat Mass Transf.* **2017**, *105*, 81–89. [[CrossRef](#)]
36. Chen, K.; Zhang, Z.; Wu, B.; Song, M.; Wu, X. An air-cooled system with a control strategy for efficient battery thermal management. *Appl. Therm. Eng.* **2024**, *236*, 121578. [[CrossRef](#)]
37. Chen, K.; Chen, Y.; Li, Z.; Yuan, F.; Wang, S. Design of the cell spacings of battery pack in parallel air-cooled battery thermal management system. *Int. J. Heat Mass Transf.* **2018**, *127*, 393–401. [[CrossRef](#)]

Disclaimer/Publisher's Note: The statements, opinions and data contained in all publications are solely those of the individual author(s) and contributor(s) and not of MDPI and/or the editor(s). MDPI and/or the editor(s) disclaim responsibility for any injury to people or property resulting from any ideas, methods, instructions or products referred to in the content.